

Uniaxial stress study of $\text{La}_{1.875}\text{Ba}_{0.125}\text{CuO}_4$ by ^{139}La NMR

I. Jakovac,¹ A. P. Dioguardi,^{2,*} M. S. Grbić,^{1,†} G. D. Gu,³
J. M. Tranquada,³ C. W. Hicks,^{4,5} M. Požek,¹ and H.-J. Grafe²

¹*Department of Physics, Faculty of Science,
University of Zagreb, Bijenička 32, Zagreb HR 10000, Croatia*

²*IFW-Dresden, Institute for Solid State Research,
PF 270116, 01171 Dresden, Germany*

³*Condensed Matter Physics and Materials Science Department,
Brookhaven National Laboratory, Upton, New York 11973, USA*

⁴*School of Physics and Astronomy,
University of Birmingham, Birmingham, B15 2TT, UK*

⁵*Max Planck Institute for Chemical Physics of Solids, 01187 Dresden, Germany*

(Dated: March 7, 2023)

Abstract

We report ^{139}La nuclear magnetic resonance measurements on a single-crystal sample of $\text{La}_{1.875}\text{Ba}_{0.125}\text{CuO}_4$ under uniaxial stress. The spin order is shown to be more robust than at $x = 0.115$ doping, however, for magnetic field H in the c direction and the stress applied along the $[110]$ direction ($\sigma_{[110]}$) the spin order transition temperature T_{SO} is rapidly suppressed. This is in stark contrast to the behavior with stress in $[100]$ direction ($\sigma_{[100]}$), which has virtually no effect on T_{SO} . For $H \parallel [1\bar{1}0]$, $\sigma_{[110]}$ stress has a weakened effect, and the rate $dT_{\text{SO}}/d\sigma_{[110]}$ is drastically reduced. Thus, $H \parallel [1\bar{1}0]$ acts as a stabilizing factor for spin-stripe order.

Also, the onset temperature of the low-temperature tetragonal crystal structure T_{LTT} is essentially unaffected by $[110]$ stress, while it decreases slowly under compression along $[100]$.

We develop a Landau free energy model and interpret our findings as an interplay of symmetry-breaking terms driven by the orientation of spins. These findings put constraints on the applicability of theoretical models for the development of spin-stripe order.

High-temperature superconductors present complex electronic behavior that has been the focus of intense research for almost four decades. One of the leading open questions is the relationship between competing electronic orders. Even though it has become clear that stripe charge order (CO) is ubiquitous in cuprates, the relationship between static charge and spin order (SO) remains incompletely understood. This is partly due to the limited number of systems in which both can be studied. The other reason is that the structural, electronic, and magnetic degrees of freedom are intertwined in these orders. Consequently, it remains a challenge to determine how they couple. In $\text{La}_{2-x}\text{Ba}_x\text{CuO}_4$ (LBCO) close to $x = 1/8$ doping, CO becomes pinned as the symmetry of the lattice changes from low-temperature orthogonal (LTO) to low-temperature tetragonal (LTT) at $T_{\text{LTT}} = 57$ K. At this doping, the SO transition temperature T_{SO} reaches its maximum value [1–4] of ≈ 40 K, while the bulk superconducting transition temperature (T_c) is strongly suppressed. T_c rapidly increases for doping away from $1/8$, even though the structural transition and CO/SO persist. It was initially hypothesized that the LTT phase, in which the structural symmetry is locally lower than in the LTO phase, was necessary for CO/SO to condense. However, Hücker et al. [5] has shown in $\text{La}_{1.875}\text{Ba}_{0.125}\text{CuO}_4$ that hydrostatic pressure above ≈ 1.85 GPa suppresses the LTO/LTT transition while CO/SO survive, which indicated that the long-range LTT

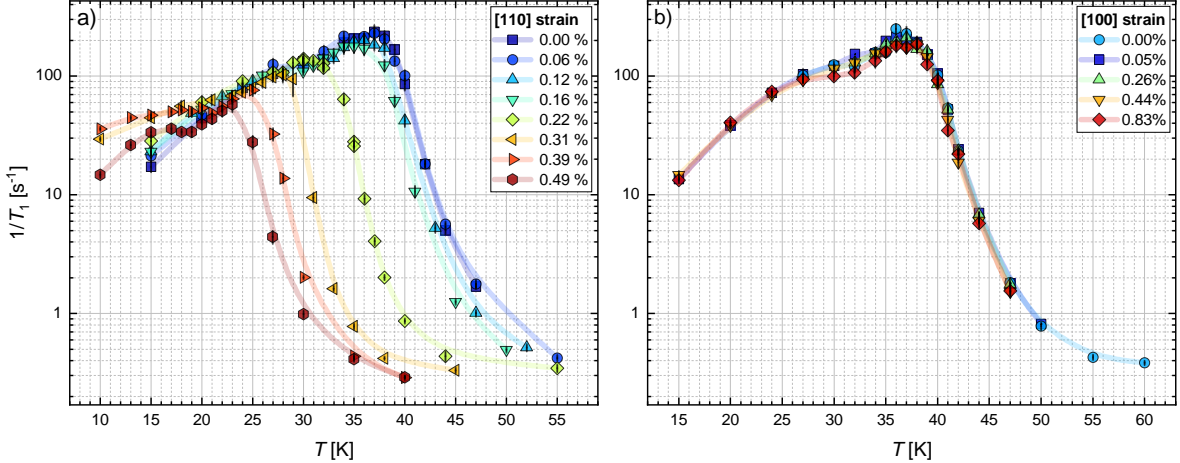


FIG. 1. Temperature dependence of ^{139}La spin-lattice relaxation rate $^{139}T_1^{-1}$ for $H \parallel c$. a) With stress applied along $[110]$ direction, T_{SO} is suppressed to lower values. b) For stress along $[100]$ direction, there is no visible change in $^{139}T_1^{-1}$ (T), even for maximum values. The values of measured $\epsilon_{[110]}$ and $\epsilon_{[100]}$ strain are shown in the legend.

structural order is not essential for CO to appear. Follow-up studies found that CO persists up to ≈ 3 GPa, but in the presence of local LTT lattice deformations [6, 7].

Similarly ambiguous connection of CO/SO to the structure is also seen in rare-earth doped La214 systems, where CO forms close to the LTO/LTT transition but with different onset temperatures. However, although these systems appear similar, upon closer inspection of their pressure-controlled phase diagrams, it becomes apparent how different they are compared to LBCO [4–12].

To understand how exactly the structural and spin orders relate in the archetypal stripe compound $\text{La}_{1.875}\text{Ba}_{0.125}\text{CuO}_4$, we studied the response of the system to uniaxial in-plane compressive stress σ using nuclear magnetic resonance (NMR) as a microscopic probe on lanthanum sites. We used the sensitivity of the ^{139}La spin-lattice relaxation rate (T_1^{-1}) to the underlying spin dynamics [13–17] and obtained $T_{\text{SO}}(\sigma)$ and $T_{\text{LTT}}(\sigma)$.

In Figs. 1 a) and b) we present the measured temperature dependence of the spin-lattice relaxation rate T_1^{-1} for stress applied along the $[110]$ and $[100]$ directions, respectively. ϵ_i denotes the strain along the i direction, obtained under σ_i . Poisson’s-ratio expansion in the transverse directions is implied. By $[110]$ we denote the direction along the diagonal of the CuO_2 square lattice with Cu in the corners, and by $[100]$ the direction along the

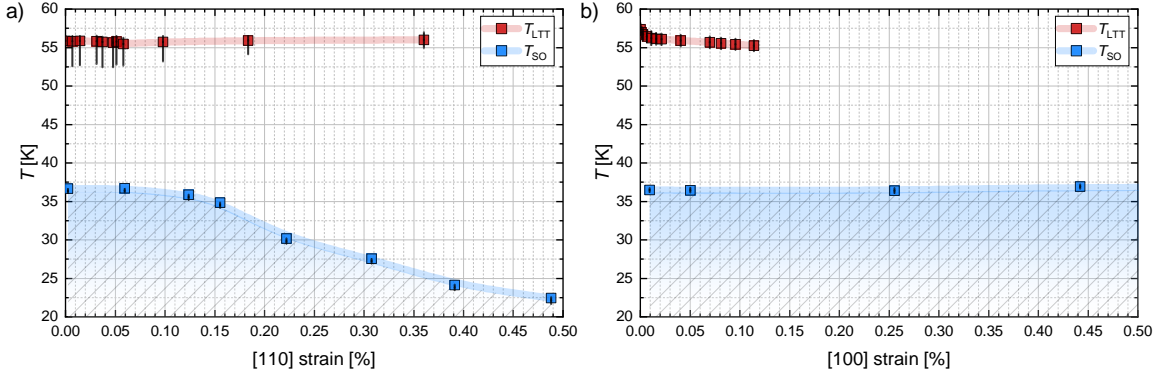


FIG. 2. Pressure-temperature phase diagram for $H \parallel c$ and a) strain along the [110] direction, and b) along the [100] direction. The data points are extracted from T_1^{-1} data of Fig. 1 and show that $\sigma_{[110]}$ reduces T_{SO} (blue), even though the onset of LTT structural phase remains the same (red). However, $\sigma_{[100]}$ does not change T_{SO} at all, while T_{LTT} shows a mild drop.

Cu–O bond. Hence, unless explicitly stated, we use labels of the crystallographic axes of the high-temperature tetragonal (HTT) phase. The magnetic field of 7 T was oriented along the crystal c axis ([001]). For $\sigma = 0$ GPa T_1^{-1} starts to increase below 55 K, as CO onsets. With cooling, slowing down of spin fluctuations cause T_1^{-1} to increase by three orders of magnitude between T_{CO} and T_{SO} , which is ≈ 37 K at $\sigma = 0$ GPa. With further cooling, T_1^{-1} decreases as the spin dynamics continues to slow down. For $H \parallel c$, such temperature dependence of ^{139}La T_1^{-1} has been shown [16, 18, 19] to be well accounted for by the electron relaxation time τ_c through the extended Bloembergen-Pound-Purcell (BPP) mechanism [20]: $T_1^{-1}(T) = \gamma^2 h_0^2 \tau_c(T) / (1 + \omega_L^2 \tau_c^2(T))$, where h_0 is the local field fluctuating at the nuclear site, γ is the gyromagnetic ratio and $\tau_c(T) = \tau_\infty \exp(E_a/k_B T)$ with an activation energy E_a . Due to the intrinsic level of disorder in the cuprates, E_a was introduced with a normal distribution of values of typical width 80 K.

When stress is applied along [110], for measured $\epsilon_{[110]}$ strain values larger than 0.1 % (which is ≈ 180 MPa, using the data from [21]), T_{SO} shifts to lower temperatures. Also, the peak value of T_1^{-1} at T_{SO} decreases. The width of the SO transition does not broaden, even at the highest stress value where T_{SO} is reduced by more than 35%, indicating a high level of strain homogeneity, and no increase of the E_a values distribution as the sample is compressed. For temperatures below T_{SO} , we see that the relaxation values under stress are not simply shifted like those for $T > T_{SO}$, but that the values smoothly connect to

the $T_1^{-1}(T)$ dependence measured at zero stress, so that $T_1^{-1}(T, \epsilon_{[110]})$ remain practically unchanged down to 20 K. As if the electronic fluctuation time τ_e , from the BPP model, is unaffected (or is reduced together with h_0) by stress, and is determined by the absolute temperature value T rather than $T - T_{\text{SO}}$. This is not what is typically observed with the suppression of a magnetic transition. One would expect that since SO is destabilized, there would be an increase in spin fluctuations, i.e., that $T_1^{-1}(T \leq T_{\text{SO}})$ would increase with $\sigma_{[110]}$.

The behavior of T_1^{-1} under $\sigma_{[110]}$ is in stark contrast to the one set by $\sigma_{[100]}$ shown in Fig. 1 b). Here, $T_1^{-1}(T)$ is essentially unaffected, even at the highest stress values. The small kink visible in both sets of data close to 25 K arises from an unusual dynamics of spin fluctuations [16].

With T_1^{-1} , we also measured the spectral features of the ^{139}La central transition (see Supplemental Material) which showed no anomalous change in linewidth or shape with temperature and stress in the region of our measurements. Hence, we conclude that samples have only undergone elastic deformation without reaching a plastic regime or cracking. Furthermore, the distribution of T_1 times, characterized by the stretching exponent s of the relaxation curves, shows a characteristic behavior observed in earlier studies [16] (see Supplemental Material).

Our results match those reported by μSR on an $x=0.115$ doped sample, for stress along a specific direction aligned 30° to the Cu-O bond [22]. There, the authors reported a drop of T_{SO} values down to 30 K for $\sigma \approx 40$ MPa, after which it reached a saturated value that barely changes up to the highest stress value of 90 MPa. However, at 1/8 doping the SO is more robust [3, 4, 23], and this is why larger stress is needed to equally suppress T_{SO} . Our results reveal that the major effect of SO suppression comes from stress along [110] direction.

To check how stress influences the LTO-LTT transition, we combine the measurements of $T_1^{-1}(T)$ and the data of voltage and capacitance measured at the strain cell. By lowering the temperature across T_{LTT} , a clear anomaly is seen in displacement (Supp. Fig. S4), caused by the change in compressibility across the structural transition [21]. The anomaly is small enough not to influence the applied stress but remains within the resolution of our measurement setup. The $T_{\text{LTT}}(\epsilon)$ dependence is also confirmed by measurements of T_1^{-1} , which shows a small peak at T_{LTT} (see Supp. Fig. S5). Similar behavior has been observed [16] at the HTT/LTO structural transition. We found that stress along [110] does

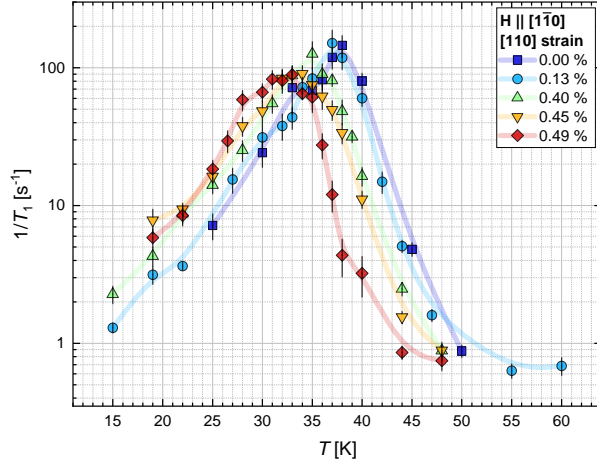


FIG. 3. Temperature dependence of $^{139}\text{T}_1^{-1}$ measured with stress $\sigma_{[110]}$ and $H \parallel [1\bar{1}0]$. The suppression of T_{SO} is greatly reduced. The legend shows the values of applied stress.

not affect the onset of the LTT phase, as is shown in Fig. 2 a). However, stress along the $[100]$ direction causes a slow but definite suppression of T_{LTT} . This is qualitatively similar to what was observed [10] in $\text{La}_{1.475}\text{Nd}_{0.4}\text{Sr}_{0.125}\text{CuO}_4$, albeit of smaller size, since there $\epsilon_{[100]}$ strain of $\approx 0.046\%$ reduced T_{LTT} from 63 K to 34 K. A reason could be that the system is close [8, 24] to a triple structural transition point rendering T_{LTT} more susceptible to external stress.

In an earlier study [16], it was found that ^{139}La T_1^{-1} shows a magnetic field-induced anisotropy connected to the relative orientation of spins [25] in the SO stripes with respect to the external magnetic field. In particular, in the SO state, T_1^{-1} is approximately an order of magnitude larger for $H \parallel [001]$ in comparison to $H \parallel [110]$ (or $[1\bar{1}0]$). This difference is not caused by the anisotropic hyperfine coupling since it would then be visible even in the paramagnetic state. Hence, the anisotropy reflects the dynamics of the SO state. To further clarify the nature of this anisotropy, we applied stress again along the $[110]$ direction, but this time with $H \parallel [1\bar{1}0]$. The results are shown in Fig. 3: for the unstressed sample, we reproduce the T_1^{-1} values within the SO phase from [16]. What is surprising, though, is that reorientation of the magnetic field drastically reduces the stress-driven suppression of T_{SO} . With $H \parallel [1\bar{1}0]$, T_{SO} is reduced to only 32 K ($\Delta T \approx 5$ K from $\sigma = 0$ GPa value) at a $[110]$ strain of 0.49 % (a stress value of ≈ 0.9 GPa). This change in T_{SO} corresponds to an overall rate of 10.2 K/% (≈ 5.63 K/GPa), which is significantly less than 27.5 K/% (≈ 15.2 K/GPa)

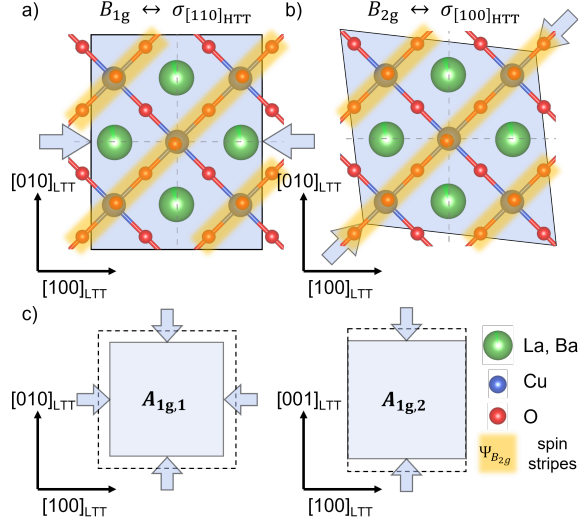


FIG. 4. Schematic of characteristic in-plane symmetry-breaking strains a) B_{1g} (orthorhombic) and b) B_{2g} (rhombic), and c) symmetric, $A_{1g,1}$ and $A_{1g,2}$, and in the LTT phase. The unstrained lattice in the foreground illustrates how the strain is applied with respect to the SO parameter $\Psi_{B_{2g}}$, symmetry-breaking order parameter $\Phi_{B_{2g}}$ (CO, octahedral tilts). B_{1g} and B_{2g} are irreducible representations of D_{4h} point group with principal axes $[100]$ and $[010]$. Strain directions are expressed in the principal axes of the HTT phase (see text).

obtained for $H \parallel c$. Clearly, the magnetic field along $[1\bar{1}0]$ reduces the effect of stress and acts as a stabilizing factor to stripe SO. This surprising result, seemingly unique to LBCO, has been implied previously [16, 25], but in this study it is directly revealed.

Another observation can be made from Fig. 3 for $\epsilon_{[110]} > 0.13\%$: in addition to the gradual shifting of T_{SO} to lower temperatures, it can be seen that the T_1^{-1} values (i.e. spin fluctuations) increase for $T < T_{SO}$. Hence, spin fluctuations now seem to depend on $T - T_{SO}$.

To address the markedly different strain dependencies of the onset temperatures T_{LTT} and T_{SO} , we consider a simple Landau free energy (LFE) model. A similar approach has led to the development of the linear two-component order parameter model [26] to explain the doping dependence of T_{LTT} in LBCO [27], stiffness constant softening observed in ultrasound experiments [28], and the out-of-plane component of magnetic moment in certain cuprate systems [29, 30]. Although such a two-component approach was prevalent, it lacked the higher-order contributions necessary to model the response to symmetry-breaking in-plane strains. Thus, the strain-related research on the iron pnictides shifted the focus to the

simpler, symmetry-defined, LFE models [31–33], which helped to elucidate how the nematic order in iron pnictides couples to the symmetry-breaking strains. The same arguments can be readily applied to characterize the observed T_{SO} suppression in $\text{La}_{1.875}\text{Ba}_{0.125}\text{CuO}_4$.

We focus on the SO transition revealed by the ^{139}La T_1^{-1} data. In the LTT phase, the $\text{La}_{1.875}\text{Ba}_{0.125}\text{CuO}_4$ crystal point group is tetragonal D_{4h} , however, owing to the octahedral tilts along $\pm[100]$ crystallographic axes, for a single CuO_2 layer the in-plane point group is reduced. We thus model the LTT phase by introducing the structural order into the D_{4h} symmetric planes. Each order parameter is associated with a specific irreducible representation characterizing its symmetry-breaking properties - in our case, both structural (Φ) and spin (Ψ) order symmetry correspond to the B_{2g} representation of the unstrained sample.

The strain tensor components can be written as an in-plane symmetric ($\epsilon_{A_{1g,1}} = \frac{1}{2}(\epsilon_{xx} + \epsilon_{yy})$, $\epsilon_{A_{1g,2}} = \epsilon_{zz}$) and antisymmetric ($\epsilon_{B_{1g}} = \frac{1}{2}(\epsilon_{xx} - \epsilon_{yy})$, $\epsilon_{B_{2g}} = \epsilon_{xy}$) linear combination [34]. The out-of-plane shear strain components ϵ_{xz} and ϵ_{yz} , which form a two-dimensional $E_g(1, 2)$ representation of the group, are absent in our measurements and can be omitted from the model. A well-founded free energy model should transform as a scalar (A_{1g}), so specific strain components are allowed to couple linearly only to the symmetry-like order parameters. The minimal LFE model is given by $F = F_\Psi + F_{\Psi\epsilon} + F_{\Psi\Phi} + F_\epsilon$, where $F_\Psi = \Psi_{B_{2g}}^2 a(T - T_{SO}) + \Psi_{B_{2g}}^4 b/2$ ($a, b > 0$) is the usual spin LFE contribution which leads to the second order phase transition, $F_{\Psi\epsilon}$ and $F_{\Psi\Phi}$ are spin-strain and spin-structure coupling terms, respectively, and F_ϵ is the elastic energy. To the lowest order in Ψ we have:

$$\begin{aligned}
F_{\Psi\epsilon} = & \alpha_1 \epsilon_{A_{1g,1}} \Psi_{B_{2g}}^2 + \alpha_2 \epsilon_{A_{1g,2}} \Psi_{B_{2g}}^2 + \\
& + \beta \epsilon_{B_{1g}}^2 \Psi_{B_{2g}}^2 + \gamma \epsilon_{B_{2g}} \Psi_{B_{2g}},
\end{aligned} \tag{1}$$

where the parameters α_1 and α_2 define the coupling strength to the symmetric, and β and γ to the antisymmetric strain. The symmetry considerations allow for a linear spin-structure coupling $F_{\Psi\Phi} = \delta \Phi_{B_{2g}} \Psi_{B_{2g}}$, where δ is the net coupling parameter. Therefore, from the model it follows that LFE minimization captures the change of $|\Psi_{B_{2g}}|$ with the structure order parameter $\Phi_{B_{2g}}$, although this does not affect the T_{SO} . However, here we will only focus on T_{SO} , since we have no data to discuss the magnitude. Finally, the elastic energy is

given by:

$$F_\epsilon = \epsilon_{A_{1g,1}}^2 (C_{11} + C_{12}) + C_{33}\epsilon_{A_{1g,2}}^2/2 + \epsilon_{B_{1g}}^2 (C_{11} - C_{12}) + 2C_{13}\epsilon_{A_{1g,1}}\epsilon_{A_{1g,2}} + 2C_{66}\epsilon_{B_{2g}}^2, \quad (2)$$

The emergence of the SO induces spontaneous strains in the lattice when cooled below T_{SO} (see Supplemental Material) which form a rhombic distortion suggesting that the external rhombic [100] stress (Fig. 4 c)) would only lead to a finite order parameter at all temperatures [34], and a crossover instead of a phase transition. However, the temperature broadening of the SO transition is not visible in our measurements, so we can conclude that the coupling to the rhombic strain is very small. On the other hand, orthorhombic strain [110] breaks an additional symmetry, introducing more terms into the electronic Hamiltonian, thus acting as a tuning parameter for the SO transition. To uncover the T_{SO} dependence on the measured strain we take applied stress as a control parameter. While below the T_{SO} , the elastic constants are renormalized by the emergent order [35], above the T_{SO} , the spontaneous strains vanish, so the strain on the sample depends only on its elastic properties. For stress along [100], the dependence of the T_{SO} is then proportional to the symmetric stress contributions:

$$\frac{\partial T_{\text{SO}}}{\partial \sigma_{[100]}} = \frac{\alpha_1(1 - \nu_{\text{in}}) - 2\alpha_2\nu_{\text{out}}}{2Y_{[100]}a}, \quad (3)$$

where ν_{in} and ν_{out} are in-plane and out-of-plane Poisson ratios, respectively, and $Y_{[100]}$ is a Young modulus along the [100] axis. The lack of any observable change in the T_{SO} measurements suggests that two symmetric stress contributions are either small or exactly cancel each other out. In contrast, when applying [110] stress to the sample, from (1), we expect the $T_{\text{SO}}(\sigma)$ dependence to be quadratic: $T_{\text{SO}}(\sigma_{[110]}) = T_{\text{SO}}^{(0)} + \alpha_{\text{eff.}}\sigma_{[110]} + \sigma_{[110]}^2\beta_{\text{eff.}}$, where $\alpha_{\text{eff.}} = \partial T_{\text{SO}}/\partial \sigma_{[110]}$ and $\beta_{\text{eff.}} = -4\beta/(G_{\text{xy}}^2 a)$, with G_{xy} denoting the in-plane shear modulus and $T_{\text{SO}}^{(0)}$ the SO transition temperature of the unstrained sample. The exact values of LFE expansion parameters α_1 , α_2 , and β determined from the effective coefficients heavily relies on a precise quantification of the sample's elastic properties. Application of the LFE model to our measurements (Fig. 5), using the elasticity data from [21] yields: $\alpha_{\text{eff.}} = -(0.3 \pm 1.0)$ K/GPa, and $\beta_{\text{eff.}} = -(21.3 \pm 4.0)$ K/GPa² for the magnetic field aligned along the c axis ([001]). The in-plane magnetic field reduces this rate drastically. Qualitatively, we expect the in-plane magnetic field $H_{[1\bar{1}0]}$ to act on the $\Psi_{B_{2g}}$ magnetic order by breaking an additional symmetry. The subsequent application of the in-plane stress is no

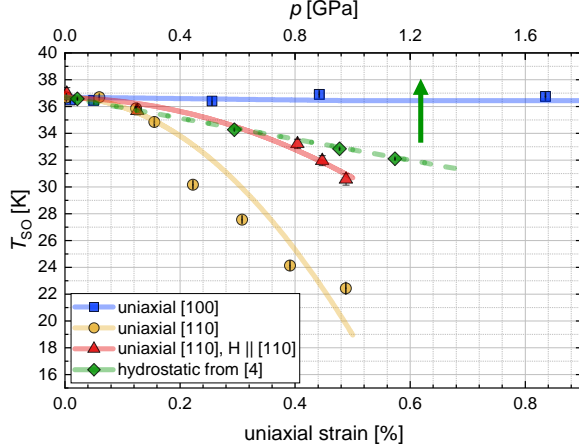


FIG. 5. T_{SO} suppression induced by different strains modeled using a simple three-parameter LFE model (see text). The hydrostatic pressure equivalent is shown on the top axis: available elasticity data suggests that $p = 2$ GPa corresponds to $\epsilon_{\text{in-plane}} \approx 1$ %. However, it is orientation-dependent ($Y_{[100]} = 233$ GPa, $Y_{[110]} = 181$ GPa). Therefore, the hydrostatic data ($p > 1$ GPa data are omitted for clarity) from [4] can be compared only qualitatively. The green dashed line is *calculated* from the other curves fitted to uniaxial strain data.

longer symmetry-breaking, so the observed suppression of the T_{SO} is diminished. Effects of the magnetic field are two-fold: the increase in in-plane magnetization, which leads to non-vanishing Zeeman contribution to the free energy, and symmetry-breaking realized by the rotation of the in-plane magnetic moments [25] through a spin-flop transition. The Zeeman contribution seems to be negligible since we do not observe a shift in T_{SO} upon field rotation from $[001]$ to $[1\bar{1}0]$ at zero strain. To address the spin rotation, we utilize an atypic two-component order parameter represented just by the B_{1g} and B_{2g} antisymmetric components:

$$\begin{pmatrix} \Psi_{B_{1g}} \\ \Psi_{B_{2g}} \end{pmatrix} = \begin{pmatrix} \Psi_0 \cos(2\phi) \\ \Psi_0 \sin(2\phi) \end{pmatrix}, \quad (4)$$

where $\Psi_0(H)$ is field-dependent order parameter magnitude, and angle ϕ describes a continuous rotation of the magnetic moments from the $[100]$ and $[010]$ directions to the $[110]$ direction. To the lowest order in Ψ , this results in the renormalization of the quadratic suppression coefficient β_{eff} upon applying $[110]$ strain, while the behavior seems unchanged under symmetric strains. The renormalized effective constant equals $\beta'_{\text{eff}}(H_{[1\bar{1}0]} = 7 \text{ T}) = -(7.0 \pm 0.7) \text{ K/GPa}^2$, which is $\approx \frac{1}{3}\beta_{\text{eff}}(H_{[001]})$.

At last, we also wish to address the T_{SO} suppression under hydrostatic pressure [4] by calculating the $T_{\text{SO}}(p)$ using our LFE model. When the strain dependence is fitted to the LFE (1), it appears the c -axis component is slightly favored ($\frac{\alpha_2}{\alpha_1} \approx 1.3$). However, overall it is the ratio of the sample's elastic constants that defines the dominant contribution in:

$$\frac{\partial T_{\text{SO}}}{\partial p} = \frac{\partial T_{\text{SO}}}{\partial \sigma_{[100]}} - \frac{\alpha_1 \nu_{\text{out}}}{Y_{[100]} a} + \frac{\alpha_2}{Y_{[001]} a}. \quad (5)$$

The first term characterizes the reaction to the in-plane symmetric $\epsilon_{A_{1g,1}}$ stress determined to be negligible. The resulting *calculated* hydrostatic suppression rate $\frac{\partial T_{\text{SO}}}{\partial p} = -(3.9 \pm 2.1) \text{ K/GPa}^2$ fits nicely to the comprehensive μSR dataset shown in Fig. 5. Data for higher pressures were omitted for clarity, but the analysis is anyway valid only until additional degrees of freedom start to contribute (e.g., interlayer coupling). It would be interesting to see how the uniaxial strain affects CO and how stress along [001] influences SO/CO. However, as such a study has various challenges, it is a topic for future work.

In summary, using ^{139}La NMR relaxation time T_1 , we present the first study of phase diagrams of stripe spin order (SO) and LTT structure onset in $\text{La}_{1.875}\text{Ba}_{0.125}\text{CuO}_4$ set by in-plane uniaxial stress (σ) in [100] and [110]. While the SO is more robust than at $x = 0.115$ doping, for $H \parallel c$ $\sigma_{[110]}$ dramatically suppresses T_{SO} and no change is found for $\sigma_{[100]}$, which limits the applicability of theoretical models. Moreover, $H \parallel [1\bar{1}0]$ stabilizes the spin order. Our results are understood as an interplay of symmetry-breaking terms driven by the spin orientation through a self-developed Landau free energy model, that simultaneously shows a good agreement with existing data on hydrostatic $T_{\text{SO}}(p)$ dependence.

The authors acknowledge the support of the Croatian Science Foundation (Grant No. IP-2018-01-2970), DFG (Grant No. DI2538/1-1), Alexander von Humboldt Foundation (Grant No. 3.4-1022249-HRV-IP), and the project CeNIKS co-funded by the Croatian Government and the EU/ERDF - Competitiveness and Cohesion Operational Programme (Grant No. KK.01.1.1.02.0013). The work at BNL was supported by the US Department of Energy, Office of Basic Energy Sciences, contract No. DOE-SC0012704. C.W.H. acknowledges support from DFG; TRR 288 - 422213477 (project A10).

* Present address: Los Alamos National Laboratory, Los Alamos, New Mexico 87545, USA.

† corresponding author: mgrbic@phy.hr

- [1] K. Kumagai, K. Kawano, I. Watanabe, K. Nishiyama, and K. Nagamine, μ SR and NMR investigations on electronic and magnetic state around $x = 0.12$ in $\text{La}_{2-x}\text{Sr}_x\text{CuO}_4$ and $\text{La}_{2-x}\text{Ba}_x\text{CuO}_4$, *Hyperfine Interactions* **86**, 473 (1994).
- [2] T. Goto, S. Kazama, K. Miyagawa, and T. Fukase, $^{63/65}\text{Cu}/^{139}\text{La}$ -NMR study on antiferromagnetic ordering in high- T_c oxides $\text{La}_{2-x}\text{Sr}_x\text{CuO}_4$ ($x \cong 0.115$) and $\text{La}_{2-x}\text{Ba}_x\text{CuO}_4$ ($x \cong 0.125$), *Journal of the Physical Society of Japan* **63**, 3494 (1994).
- [3] M. Hücker, M. v. Zimmermann, G. D. Gu, Z. J. Xu, J. S. Wen, G. Xu, H. J. Kang, A. Zheludev, and J. M. Tranquada, Stripe order in superconducting $\text{La}_{2-x}\text{Ba}_x\text{CuO}_4$ ($0.095 \leq x \leq 0.155$), *Physical Review B* **83**, 104506 (2011).
- [4] Z. Guguchia, R. Khasanov, A. Shengelaya, E. Pomjakushina, S. J. L. Billinge, A. Amato, E. Morenzoni, and H. Keller, Cooperative coupling of static magnetism and bulk superconductivity in the stripe phase of $\text{La}_{1.875}\text{Ba}_{0.125}\text{CuO}_4$: Pressure- and doping-dependent studies, *Physical Review B* **94**, 214511 (2016).
- [5] M. Hücker, M. v. Zimmermann, M. Debessai, J. S. Schilling, J. M. Tranquada, and G. D. Gu, Spontaneous symmetry breaking by charge stripes in the high pressure phase of superconducting $\text{La}_{1.875}\text{Ba}_{0.125}\text{CuO}_4$, *Physical Review Letters* **104**, 057004 (2010).
- [6] G. Fabbris, M. Hücker, G. D. Gu, J. M. Tranquada, and D. Haskel, Local structure, stripe pinning, and superconductivity in $\text{La}_{1.875}\text{Ba}_{0.125}\text{CuO}_4$ at high pressure, *Physical Review B* **88**, 060507 (2013).
- [7] G. Fabbris, M. Hücker, G. D. Gu, J. M. Tranquada, and D. Haskel, Combined single crystal polarized XAFS and XRD at high pressure: probing the interplay between lattice distortions and electronic order at multiple length scales in high t_c cuprates, *High Pressure Research* **36**, 348 (2016).
- [8] M. K. Crawford, R. L. Harlow, S. Deemyad, V. Tissen, J. S. Schilling, E. M. McCarron, S. W. Tozer, D. E. Cox, N. Ichikawa, S. Uchida, and Q. Huang, High-pressure study of structural phase transitions and superconductivity in $\text{La}_{1.48}\text{Nd}_{0.4}\text{Sr}_{0.12}\text{CuO}_4$, *Physical Review B* **71**, 104513 (2005).
- [9] B. Simović, M. Nicklas, P. C. Hammel, M. Hücker, B. Büchner, and J. D. Thompson, Interplay between freezing and superconductivity in the optimally doped $\text{La}_{1.65}\text{Eu}_{0.2}\text{Sr}_{0.15}\text{CuO}_4$ under hydrostatic pressure, *Europhysics Letters* **66**, 722 (2004).
- [10] T. J. Boyle, M. Walker, A. Ruiz, E. Schierle, Z. Zhao, F. Boschini, R. Sutarto, T. D. Boyko,

- W. Moore, N. Tamura, F. He, E. Weschke, A. Gozar, W. Peng, A. C. Komarek, A. Damascelli, C. Schüßler-Langeheine, A. Frano, E. H. da Silva Neto, and S. Blanco-Canosa, Large response of charge stripes to uniaxial stress in $\text{La}_{1.475}\text{Nd}_{0.4}\text{Sr}_{0.125}\text{CuO}_4$, *Physical Review Research* **3**, L022004 (2021).
- [11] S. Arumugam, N. Môri, N. Takeshita, H. Takashima, T. Noda, H. Eisaki, and S. Uchida, Competition of static stripe and superconducting phases in $\text{La}_{1.48}\text{Nd}_{0.4}\text{Sr}_{0.12}\text{CuO}_4$ controlled by pressure, *Physical Review Letters* **88**, 247001 (2002).
- [12] N. Takeshita, T. Sasagawa, T. Sugioka, Y. Tokura, and H. Takagi, Gigantic anisotropic uniaxial pressure effect on superconductivity within the CuO_2 plane of $\text{La}_{1.64}\text{Eu}_{0.2}\text{Sr}_{0.16}\text{CuO}_4$: Strain control of stripe criticality, *Journal of the Physical Society of Japan* **73**, 1123 (2004).
- [13] A. Arsenault, S. K. Takahashi, T. Imai, W. He, Y. S. Lee, and M. Fujita, ^{139}La NMR investigation of the charge and spin order in a $\text{La}_{1.885}\text{Sr}_{0.115}\text{CuO}_4$ single crystal, *Physical Review B* **97**, 064511 (2018).
- [14] P. M. Singer, A. W. Hunt, A. F. Cederström, and T. Imai, Systematic ^{63}Cu NQR study of the stripe phase in $\text{La}_{1.6-x}\text{Nd}_{0.4}\text{Sr}_x\text{CuO}_4$ for $0.07 \leq x \leq 0.25$, *Physical Review B* **60**, 15345 (1999).
- [15] P. M. Singer, A. W. Hunt, and T. Imai, ^{63}Cu NQR evidence for spatial variation of hole concentration in $\text{La}_{2-x}\text{Sr}_x\text{CuO}_4$, *Physical Review Letters* **88**, 047602 (2002).
- [16] S.-H. Baek, Y. Utz, M. Hücker, G. D. Gu, B. Büchner, and H.-J. Grafe, Magnetic field induced anisotropy of ^{139}La spin-lattice relaxation rates in stripe ordered $\text{La}_{1.875}\text{Ba}_{0.125}\text{CuO}_4$, *Physical Review B* **92**, 155144 (2015).
- [17] P. M. Singer, A. Arsenault, T. Imai, and M. Fujita, ^{139}La NMR investigation of the interplay between lattice, charge, and spin dynamics in the charge-ordered high- T_c cuprate $\text{La}_{1.875}\text{Ba}_{0.125}\text{CuO}_4$, *Physical Review B* **101**, 174508 (2020).
- [18] B. J. Suh, P. C. Hammel, M. Hücker, B. Büchner, U. Ammerahl, and A. Revcolevschi, Spin dynamics in the low-temperature tetragonal phase of $\cong \frac{1}{8}$ doped single crystal $\text{La}_{1.67}\text{Eu}_{0.2}\text{Sr}_{0.13}\text{CuO}_4$, *Physical Review B* **61**, R9265 (2000).
- [19] N. J. Curro, P. C. Hammel, B. J. Suh, M. Hücker, B. Büchner, U. Ammerahl, and A. Revcolevschi, Inhomogeneous low frequency spin dynamics in $\text{La}_{1.65}\text{Eu}_{0.2}\text{Sr}_{0.15}\text{CuO}_4$, *Physical Review Letters* **85**, 642 (2000).
- [20] N. Bloembergen, E. M. Purcell, and R. V. Pound, Relaxation effects in nuclear magnetic

- resonance absorption, *Physical Review* **73**, 679 (1948).
- [21] M. Nohara, T. Suzuki, Y. Maeno, T. Fujita, I. Tanaka, and H. Kojima, Unconventional lattice stiffening in superconducting $\text{La}_{2-x}\text{Sr}_x\text{CuO}_4$ single crystals, *Physical Review B* **52**, 570 (1995).
- [22] Z. Guguchia, D. Das, C. N. Wang, T. Adachi, N. Kitajima, M. Elender, F. Brückner, S. Ghosh, V. Grinenko, T. Shiroka, M. Müller, C. Mudry, C. Baines, M. Bartkowiak, Y. Koike, A. Amato, J. M. Tranquada, H.-H. Klauss, C. W. Hicks, and H. Luetkens, Using uniaxial stress to probe the relationship between competing superconducting states in a cuprate with spin-stripe order, *Physical Review Letters* **125**, 097005 (2020).
- [23] W. Schottenhamel, *Aufbau eines hochauflösenden Dilatometers und einer hydrostatischen SQUID-Druckzelle sowie Untersuchungen an korrelierten Übergangsmetalloxiden*, Ph.D. thesis, Technische Universität Dresden (2016).
- [24] M. K. Crawford, R. L. Harlow, E. M. McCarron, W. E. Farneth, J. D. Axe, H. Chou, and Q. Huang, Lattice instabilities and the effect of copper-oxygen-sheet distortions on superconductivity in doped La_2CuO_4 , *Physical Review B* **44**, 7749 (1991).
- [25] M. Hücker, G. D. Gu, and J. M. Tranquada, Spin susceptibility of underdoped cuprate superconductors: Insights from a stripe-ordered crystal, *Physical Review B* **78**, 214507 (2008).
- [26] N. Plakida and V. Shakhmatov, Structural phase transitions in superconducting LaSrCuO compounds, *Physica C: Superconductivity* **153-155**, 233 (1988).
- [27] Y. Ishibashi, The phase diagram of $\text{La}_{2-x}\text{Ba}_x\text{CuO}_4$, *Journal of the Physical Society of Japan* **59**, 800 (1990).
- [28] A. Migliori, W. M. Visscher, S. Wong, S. E. Brown, I. Tanaka, H. Kojima, and P. B. Allen, Complete elastic constants and giant softening of c_{66} in superconducting $\text{La}_{1.86}\text{Sr}_{0.14}\text{CuO}_4$, *Physical Review Letters* **64**, 2458 (1990).
- [29] M. Hücker, V. Kataev, J. Pommer, U. Ammerahl, A. Revcolevschi, J. M. Tranquada, and B. Büchner, Dzyaloshinsky-Moriya spin canting in the low-temperature tetragonal phase of $\text{La}_{2-x-y}\text{Eu}_y\text{Sr}_x\text{CuO}_4$, *Physical Review B* **70**, 214515 (2004).
- [30] B. Keimer, R. J. Birgeneau, A. Cassanho, Y. Endoh, M. Greven, M. A. Kastner, and G. Shirane, Soft phonon behavior and magnetism at the low temperature structural phase transition of $\text{La}_{1.65}\text{Nd}_{0.35}\text{CuO}_4$, *Zeitschrift für Physik B Condensed Matter* **91**, 373 (1993).
- [31] A. Togo, F. Oba, and I. Tanaka, First-principles calculations of the ferroelastic transition between rutile-type and CaCl_2 -type SiO_2 at high pressures, *Physical Review B* **78**, 134106

- (2008).
- [32] X. Lu, K.-F. Tseng, T. Keller, W. Zhang, D. Hu, Y. Song, H. Man, J. T. Park, H. Luo, S. Li, A. H. Nevidomskyy, and P. Dai, Impact of uniaxial pressure on structural and magnetic phase transitions in electron-doped iron pnictides, *Physical Review B* **93**, 134519 (2016).
 - [33] J.-H. Chu, H.-H. Kuo, J. G. Analytis, and I. R. Fisher, Divergent nematic susceptibility in an iron arsenide superconductor, *Science* **337**, 710 (2012).
 - [34] M. S. Ikeda, T. Worasaran, J. C. Palmstrom, J. A. W. Straquadine, P. Walmsley, and I. R. Fisher, Symmetric and antisymmetric strain as continuous tuning parameters for electronic nematic order, *Physical Review B* **98**, 245133 (2018).
 - [35] N. Plakida, *High-Temperature Cuprate Superconductors: Experiment, Theory, and Applications*, Springer Series in Solid-State Sciences (Springer Berlin Heidelberg, 2010).
 - [36] G. Gu, M. Hücker, Y.-J. Kim, J. Tranquada, Q. Li, and A. Moodenbaugh, Single-crystal growth and superconductivity of $(\text{La}_{1-x}\text{Sr}_x)_2\text{CaCu}_2\text{O}_{6+\delta}$, *Journal of Crystal Growth* **287**, 318 (2006).
 - [37] C. W. Hicks, M. E. Barber, S. D. Edkins, D. O. Brodsky, and A. P. Mackenzie, Piezoelectric-based apparatus for strain tuning, *Review of Scientific Instruments* **85**, 065003 (2014), <https://doi.org/10.1063/1.4881611>.
 - [38] T. Hashimoto and A. Ikushima, Mechanical properties of stycast-1266 at low temperatures, *Review of Scientific Instruments* **51**, 378 (1980).
 - [39] D. C. Johnston, Stretched exponential relaxation arising from a continuous sum of exponential decays, *Phys. Rev. B* **74**, 184430 (2006).
 - [40] V. F. Mitrović, M.-H. Julien, C. de Vaulx, M. Horvatić, C. Berthier, T. Suzuki, and K. Yamada, Similar glassy features in the ^{139}La NMR response of pure and disordered $\text{La}_{1.88}\text{Sr}_{0.12}\text{CuO}_4$, *Phys. Rev. B* **78**, 014504 (2008).

SUPPLEMENTARY NOTE 1: Technical details of the measurement setup

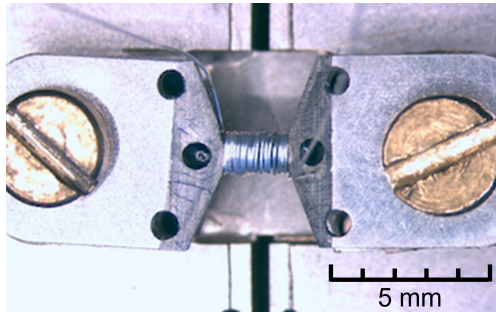


FIG. 6. NMR coil with the sample in the uniaxial cell.

In Fig. 6, we show a part of our measurement setup with the sample and an NMR coil in a strain cell. The $\text{La}_{1.875}\text{Ba}_{0.125}\text{CuO}_4$ single crystal was grown with the traveling solvent floating-zone method described in Ref. [36]. Samples were first properly aligned by Laue scattering and cut along the specific crystallographic directions in the high-temperature tetragonal phase. In our measurements, we employ a uniaxial strain cell driven by a stack of piezoelectric transducers designed to work in a wide range of temperatures [37]. Each sample was mounted on titanium holders and fixed by 2850FT Stycast epoxy (cat. 9). We cooled down the apparatus to $T = 60$ K in a continuous flow cryostat with the piezo stacks shorted. All subsequent temperature changes were performed by holding the piezo stack voltages fixed. The induced strain was measured using a calibrated capacitive dilatometer in conjunction with the Andeen-Hagerling 2550A ultra-precision capacitance bridge. The initial NMR measurements and capacitive dilatometer readings suggest that the strain due to the strain cell's thermal expansion (contraction) is negligible due to the specific design of the strain cell. The applied stress was varied [37] by applying voltages $V_{\text{in.}} = \pm 200$ V, $V_{\text{out.}} = \pm 200$ V, with the outer piezo stacks and inner piezo stacks driven independently. We were able to induce a strain up to $\epsilon \approx 1\%$, depending on the sample orientation and dimensions.

We used a simplified model introduced elsewhere [37] to gauge the uniaxial stress transferred to the sample:

$$\sigma_a = \frac{Y_a \Delta L}{2\lambda + l_0},$$

where Y_a is a Young modulus along a given axis, ΔL is a measured displacement change, and

l_0 is the initial size of the sample along the strained dimension. The parameter λ , defining a length scale over which the stress is transferred to the sample, is given by:

$$\lambda = \sqrt{\frac{Y_a t d}{2G}},$$

where t and d denote the thickness of the sample and epoxy, respectively, and G is a shear strain modulus of the epoxy. We assume the epoxy to be an isotropic elastic material, and thus $G = Y_{\text{epoxy}}/(2 + 2\nu)$ where we take the Young modulus and Poisson ratio to be $Y_{\text{epoxy}} = 15$ GPa and $\nu = 0.3$ [38]. Unfortunately, the elastic constants for LBCO at 1/8 doping were not determined at cryogenic temperatures. However, data for similar compounds such as LSCO [21] or LCO [28] corresponds to the transferred stress on the order of ≈ 1.5 GPa at the highest applied voltages. At last, we have calculated the relative strain loss to the epoxy:

$$\eta_{\text{loss}} = \frac{\Delta L - \Delta l_{\text{sample}}}{\Delta L} = \frac{2\lambda}{2\lambda + l_0},$$

which amounts to the loss $\eta_{\text{loss}} \approx 0.4 - 0.5$ for all our samples.

SUPPLEMENTARY NOTE 2: NMR data acquisition information

NMR data were collected on a central ($+1/2 \leftrightarrow -1/2$) transition of the ^{139}La spectra using a Tecmag spectrometer with a Hahn echo pulse sequence $\pi/2 - \tau - \pi$. Typical $\pi/2$ pulse length was $0.5 \mu\text{s}$ and $\tau = 17 \mu\text{s}$, while pulse power was 0.5 W. With the magnetic field of 7 T T_1^{-1} was measured at frequency $\omega_L = 42.18$ MHz.

In Fig. 7, we show temperature corrected ^{139}La NMR spectra with uniaxial strain applied along $[110]$ axis. We have observed no significant change in spectral width, and frequency with the applied $[100]$ or $[110]$ uniaxial strain. We attribute a noticeable decrease in the signal intensity across T_{SO} to the enhanced longitudinal spin fluctuations near the spin-order transition. The spectra differ at the intermediate temperatures due to varying extent of the T_{SO} suppression with the applied $[110]$ uniaxial strain. At low temperatures ($T < 28$ K), when spin fluctuations under different strains become comparable (Fig. 1 a)), the lineshapes coincide again. The effect is most noticeable at $T = 34$ K. Here, at low strains, the spectrum is measured precisely, or a bit below T_{SO} , and thus, the spectral intensity is significantly diminished. The change in the signal intensity is hardly noticeable at the highest strains,

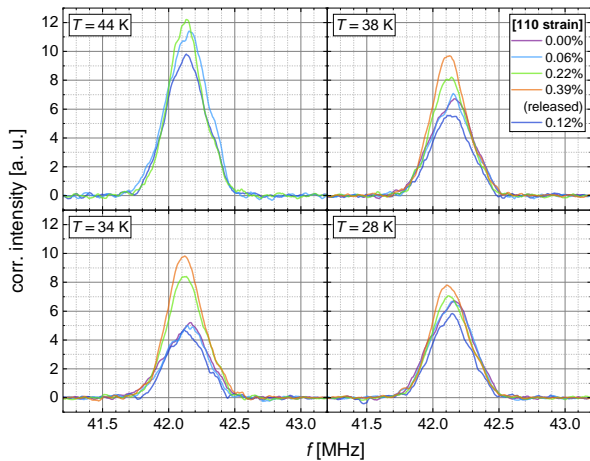


FIG. 7. ^{139}La NMR spectra (central transition) under different [110] uniaxial strains, at chosen temperatures above and below T_{SO} .

but becomes pronounced once again when the strain is released. When the strain is released, the original lineshape is recovered.

Spin-lattice relaxation rates were determined by a saturation-pulse recovery sequence, after which the data were fit to a relaxation curve $f(t) = (1/84)e^{-(t/T_1)^s} + (3/44)e^{-(6t/T_1)^s} + (75/364)e^{-(15t/T_1)^s} + (1225/1716)e^{-(28t/T_1)^s}$. The phenomenological stretching exponent s gives insight into the distribution of the relaxation times T_1 . The $s \geq 0.5$ implies the Gaussian T_1 distribution on a logarithmic scale with FWHM across an order of magnitude and $T_1 \approx T_{1,\text{median}}$. When $s < 0.5$, the distribution widens drastically, and the fitted T_1 no longer represents the median of the distribution [39].

To accurately interpret the measured T_1 NMR relaxation data, we shall discuss the temperature and strain dependence of the fitted stretch exponent s (Fig. 8). When we approach the spin-order transition temperature T_{SO} for a given strain, the s dips abruptly. This behavior has already been observed in various cuprate systems, which exhibit a glassy type spin-order transition [17, 40]. We can see that the spatial distribution of T_1 times broadens significantly, but the stretch exponent stays predominantly larger than the threshold value of $s \approx 0.5$. It is, therefore, appropriate to analyze the fitted T_1 values as they always stay within $\sim 20\%$ of the distribution median. Conversely, it is justifiable to take a fixed value of s to facilitate the interpretation of the fitted T_1 values [19].

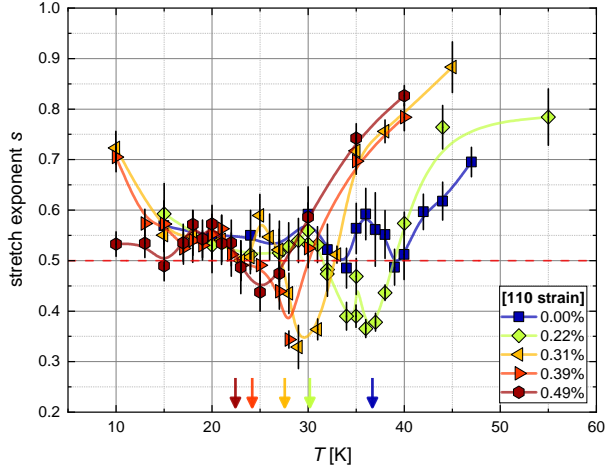


FIG. 8. Stretching exponent s fitted to our measurements. For clarity, we show only a subset of measured [110] strains with interpolated cubic splines as guides to the eye. Change in s close to the transition temperature T_{SO} is undoubtedly visible, and the strain dependence of the observed dip follows the same pattern as the T_1 data. The color-coded arrows mark T_{SO} at respective strain.

SUPPLEMENTARY NOTE 3: Observing the LTO-LTT transition

Although the capacitive dilatometer of our strain cell has lower sensitivity than custom thermal-expansion measurement setups, it was sufficiently sensitive to detect a first-order LTO-LTT structural transition. We performed an exhaustive set of temperature sweeps at different uniaxial strains to characterize a change in the structural transition temperature T_{LTT} . We used two sweep rates, $r_1 = 1$ K/min and $r_2 = 0.5$ K/min, with each dataset measured for both cooling and warming, while the piezo stack voltage was held constant. Therefore, the observed displacement change should only come from the thermal expansion of the strain cell or the change in the sample's elastic properties. With the former being negligible in the measured temperature range, we can easily follow a structural transition as we increase the uniaxial stress on the sample.

When applying [110] uniaxial stress, the change in T_{LTT} is absent or too small to be revealed by this method. In contrast, with the application of [100] stress sample displays a gradual, linear suppression of the T_{LTT} . Arguably, [100] stress promotes orthorhombicity and suppresses the transition to the LTT phase.

To confirm our dilatometry measurements, we look for the LTO-LTT structural transition

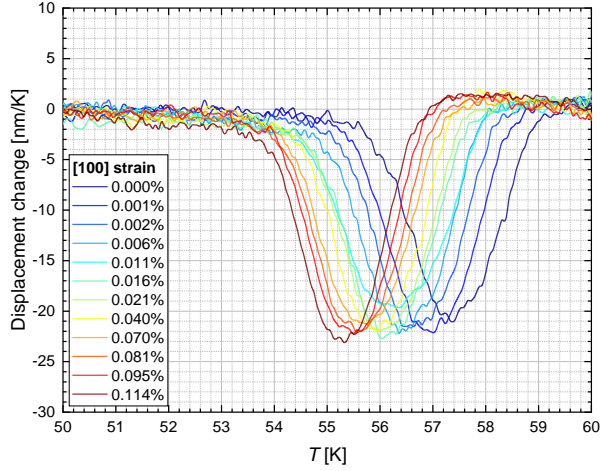


FIG. 9. The anomaly in displacement change ($\Delta L/\Delta T$) of the strain cell measured in cooling ($r = 1$ K/min) for different applied stresses along [100] direction. The anomaly temperature coincides with the structural transition temperature $T_{\text{LTT}} = 57.5$ K at zero applied stress. For increased strain values shown in the legend, the anomaly shifts to a lower temperature of 55.5 K.

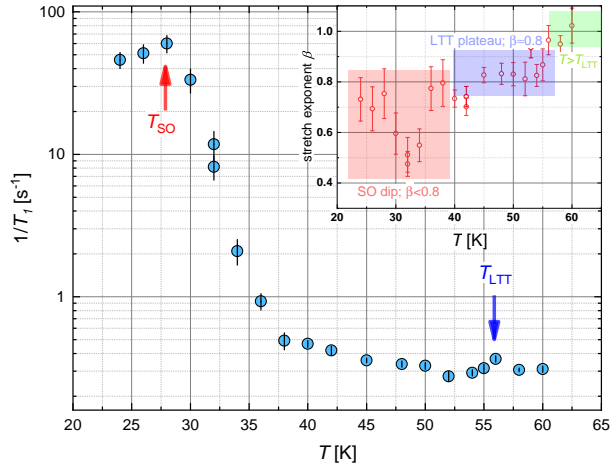


FIG. 10. Wide temperature range T_1 measurement at uniaxial strain $\epsilon_{[110]} = 0.4\%$ reveals an anomaly at tentative $T_{\text{LTT}} \approx 56$ K. The anomaly also coincides with a smaller dip in stretch exponent s , which drops to $s = 0.5$ when T_{SO} is approached.

in our T_1 NMR measurements. Using uniaxial stress along the [110] direction, we suppress the spin transition down to $T_{\text{SO}} \approx 28$ K, revealing a discernible anomaly at $T_{\text{LTT}} \approx 56$ K which roughly coincides with the LTO-LTT transition. A similar feature was already observed in LESCO [9] where the structural transition is separated from T_{SO} at zero strain. In

addition to the slight increase in T_1^{-1} relaxation rate, there is a discernible dip, LTT plateau in 10, in stretch exponent s at T_{LTT} , which implies a broader spatial distribution of the relaxation times T_1 . This is consistent with the mixed-phase associated with the first-order structural transition.

SUPPLEMENTARY NOTE 4: Calculation of the Landau free energy model

In the uniaxial strain experiment, it is advantageous to take the external stress applied on the sample as an independent variable. However, it is the induced strain that governs the suppression of the spin order transition temperature T_{SO} ; so it is essential to handle the stress-strain conversion properly. In cuprates, and especially for LBCO and LSCO [21, 28], the elastic constants are given along the crystallographic axes of the high-temperature (HTT) phase. Suppose we wish to construct our free energy model in the LTT phase where the spin order sets in. In that case, we must transform the components of the stiffness matrix \mathbf{C} using the familiar fourth-order tensor rotation formula:

$$C'_{ijkl} = c_i c_j c_k c_l C_{ijkl}, \quad (6)$$

where coefficients c_i, c_j, c_k, c_l represent directional cosines along i, j, k, l axes. In the transformation from the HTT to the LTT crystallographic axes, we can limit ourselves to the rotation about the z axis ($\theta = \pm 45^\circ$). Equation 6 can then be condensed into a 6×6 rotation matrix:

$$\mathbf{R} = \begin{pmatrix} c^2 & s^2 & 0 & 0 & 0 & 2cs \\ s^2 & c^2 & 0 & 0 & 0 & -2cs \\ 0 & 0 & 1 & 0 & 0 & 0 \\ 0 & 0 & 0 & c & s & 0 \\ 0 & 0 & 0 & -s & c & 0 \\ -cs & cs & 0 & 0 & 0 & c^2 - s^2 \end{pmatrix}, \quad \begin{matrix} c \equiv \cos \theta \\ s \equiv \sin \theta \end{matrix}, \quad (7)$$

which acts on a stiffness tensor $\mathbf{C}^{(\text{LTT})} = \mathbf{R}\mathbf{C}^{(\text{HTT})}\mathbf{R}^T$. At last, to make the expressions more convenient to analyze and use, we replace the stiffness constant by utilizing the relation:

$$\begin{aligned} (\mathbf{C}^{(\text{HTT,LTT})})^{-1} &= \mathbf{S}^{(\text{HTT,LTT})} \\ &= \begin{pmatrix} \frac{1}{Y_{[100]}} & -\frac{\nu_{\text{in}}}{Y_{[100]}} & -\frac{\nu_{\text{out}}}{Y_{[100]}} & 0 & 0 & 0 \\ -\frac{\nu_{\text{in}}}{Y_{[100]}} & \frac{1}{Y_{[100]}} & -\frac{\nu_{\text{out}}}{Y_{[100]}} & 0 & 0 & 0 \\ -\frac{\nu_{\text{out}}}{Y_{[100]}} & -\frac{\nu_{\text{out}}}{Y_{[100]}} & \frac{1}{Y_{[001]}} & 0 & 0 & 0 \\ 0 & 0 & 0 & \frac{1}{G_{zx}} & 0 & 0 \\ 0 & 0 & 0 & 0 & \frac{1}{G_{zx}} & 0 \\ 0 & 0 & 0 & 0 & 0 & \frac{1}{G_{xy}} \end{pmatrix}, \end{aligned} \quad (8)$$

where the elastic compliance matrix \mathbf{S} is given in terms of Young and shear moduli ($Y_{[100]} = 233$ GPa, $Y_{[001]} = 176$ GPa, $G_{zx} \approx G_{xy} = 66.4$ GPa) and Poisson ratios ($\nu_{\text{in}} = 0.18$, $\nu_{\text{out}} = 0.27$). In this work, we use elastic stiffness constants given for the LTT phase when setting up the model but then express the results using the elastic parameters of the HTT lattice. The reason for this is twofold: the sample is oriented and glued into the strain cell with respect to the HTT axes, and we can readily use the elastic data from other sources to gauge the induced strain and expected T_{SO} suppression.

To accentuate the role of the symmetry-breaking stress on the transition, we use an (anti) symmetrized strain components $\epsilon_{A_{1g,1}} = \frac{1}{2}(\epsilon_{xx} + \epsilon_{yy})$, $\epsilon_{A_{1g,2}} = \epsilon_{zz}$ and $\epsilon_{B_{1g}} = \frac{1}{2}(\epsilon_{xx} - \epsilon_{yy})$, $\epsilon_{B_{2g}} = \epsilon_{xy}$. From here, we construct a model taking into account five contributions to free energy:

$$\begin{aligned} F &= F_{\Psi} + F_{\Psi\epsilon} + F_{\Psi\Phi} + F_{\epsilon} + F_{\sigma} \\ F_{\Psi} &= \Psi_{B_{2g}}^2 a (T - T_{\text{SO}}) + \Psi_{B_{2g}}^4 b/2, \\ F_{\Psi\epsilon} &= \alpha_1 \epsilon_{A_{1g,1}} \Psi_{B_{2g}}^2 + \alpha_2 \epsilon_{A_{1g,2}} \Psi_{B_{2g}}^2 + \beta \epsilon_{B_{1g}}^2 \Psi_{B_{2g}}^2 + \gamma \epsilon_{B_{2g}} \Psi_{B_{2g}}, \\ F_{\Psi\Phi} &= \delta \Phi_{B_{2g}} \Psi_{B_{2g}} \\ F_{\epsilon} &= \epsilon_{A_{1g,1}}^2 (C_{11} + C_{12}) + C_{33} \epsilon_{A_{1g,2}}^2 / 2 + \epsilon_{B_{1g}}^2 (C_{11} - C_{12}) + 2C_{13} \epsilon_{A_{1g,1}} \epsilon_{A_{1g,2}} + 2C_{66} \epsilon_{B_{2g}}^2, \\ F_{\sigma} &= -\sigma \cdot \epsilon, \end{aligned} \quad (9)$$

where $\Psi_{B_{2g}}^2$ represents an emergent spin order which transforms as a B_{2g} irreducible representation of a D_{4h} point group, and $\Phi_{B_{2g}}$, a structural order parameter, taken to be temperature independent for reasons listed in the article. All the contributions contain the lowest order

terms in order parameters, with coupling constants expressed as α_1 , α_2 , β , γ and δ . a and b ($a, b > 0$) are the standard Landau expansion parameters. The last, elastic energy contribution, sets the strains as a function of the applied uniaxial stress. At the minimum of the total free energy in the absence of the spin/structural order, F_σ must be precisely equal to the quadratic form in strains F_ϵ .

We can find the equilibrium strain as a solution to the set of minimization conditions $\frac{\partial F}{\partial \epsilon_i} = 0$ given for all the symmetric and antisymmetric combinations of the strain. Evaluating the solution at $\sigma_{[100]} = 0$ GPa or $\sigma_{[110]} = 0$ GPa implies the emergence of spontaneous strains when the system enters a spin-ordered phase:

$$\begin{aligned}\epsilon_{A_{1g};1} &= \frac{\Psi_{B_{2g}}^2 [(\nu_{\text{in}} - 1)\alpha_1 + 2\nu_{\text{out}}\alpha_2]}{2Y_{[100]}}, \\ \epsilon_{A_{1g};2} &= \frac{\Psi_{B_{2g}}^2 (-Y_{[100]}\alpha_2 + Y_{[001]}\nu_{\text{out}}\alpha_1)}{Y_{[100]}Y_{[001]}}, \\ \epsilon_{B_{2g}} &= -\frac{\Psi_{B_{2g}}\gamma(\nu_{\text{in}} + 1)}{8Y_{[100]}}, \\ \epsilon_{B_{1g}} &= \epsilon_{E_g(1)} = \epsilon_{E_g(2)} = 0.\end{aligned}\tag{10}$$

Introduction of the equilibrium strain into the free energy model and minimization with respect to the order parameter $\Psi_{B_{2g}}$ results in a third order polynomial in $\Psi_{B_{2g}}$, with a single real solution. One may argue that the complex solutions to the order parameters are standard; however, we must disregard them as we have taken $\Psi_{B_{2g}}$ as the order magnitude, and we have allowed for a linear coupling in $\Psi_{B_{2g}}$. Therefore, such a solution would yield a non-physical complex free energy.

The real solution for the stress $\sigma_{[100]}$ applied along $[100]$ axis, implies that the T_{SO} is suppressed in a linear fashion:

$$\frac{\partial T_{\text{SO}}}{\sigma_{[100]}} = \frac{(1 - \nu_{\text{in}})\alpha_1}{2Y_{[100]}a} - \frac{\nu_{\text{out}}\alpha_2}{Y_{[100]}a} \equiv f(\alpha_1, \alpha_2).\tag{11}$$

Here, we observe that coupling constants β and γ are absent; thus, only the induced symmetric strains govern the suppression. We will encounter this expression multiple times, and therefore define it as a function $f(\alpha_1, \alpha_2)$. We purposefully consider $Y_{[100]}$ as a constant in $f(\alpha_1, \alpha_2)$ since the following expressions can always be expressed using exactly $Y_{[100]}$, irrespective of the direction of the applied stress. As noted in the article, we do not observe a measurable change in T_{SO} with this sample orientation, so that we can approximate

$f(\alpha_1, \alpha_2) \approx 0$ K/GPa. When the stress $\sigma_{[110]}$ is applied to the sample, the T_{SO} suppression is quadratic in $\sigma_{[110]}$. The linear term has the exact form as with the $\sigma_{[100]}$ stress, while the quadratic part depends on the sample's shear modulus G_{xy} :

$$\Delta T_{\text{SO}}(\sigma_{[110]}) = f(\alpha_1, \alpha_2)\sigma_{[110]} - \frac{4\beta}{G_{xy}^2 a} \sigma_{[110]}^2 \approx -\frac{4\beta}{G_{xy}^2 a} \sigma_{[110]}^2. \quad (12)$$

The T_{SO} suppression under hydrostatic regime can also be expressed using $f(\alpha_1, \alpha_2)$, so we can reduce the dependence to:

$$\frac{\partial T_{\text{SO}}}{\partial p} = f(\alpha_1, \alpha_2) - \frac{\nu_{\text{out}}\alpha_1}{Y_{[100]}a} + \frac{\alpha_2}{Y_{[001]}a} \approx -\frac{\nu_{\text{out}}\alpha_1}{Y_{[100]}a} + \frac{\alpha_2}{Y_{[001]}a}. \quad (13)$$

Note that the symmetric strain contribution $f(\alpha_1, \alpha_2)$ is present in both expressions for the T_{SO} suppression rate. However, as discussed earlier, it seems to be negligible.

Now, we turn our attention to the model extension, which describes the effect of the external magnetic field. The standard way of treating the in-plane external magnetic field is to include a Zeeman contribution $F_{\text{Zeeman}} = \mu\mathbf{H} \cdot \mathbf{m}(\Psi_{B_{2g}})$, where $\mathbf{m}(\Psi_{B_{2g}})$ represents a magnetic moment associated with the order parameter $\Psi_{B_{2g}}$. Unfortunately, it is immediately evident that such a contribution would lead to a change in T_{SO} at all strains. In our model, we propose a two-component order parameter by introducing in-plane order parameters which are defined by different symmetry properties: $\Psi_{B_{1g}}$ transforms as B_{1g} , and $\Psi_{B_{2g}}$ transforms as B_{2g} representation of the D_{4h} point group. We proceed to write down the Landau model in the absence of strain up to the fourth-order invariants:

$$F_{\Psi} = a(T - T_{\text{SO}})(\Psi_{B_{1g}}^2 + \Psi_{B_{2g}}^2) + \frac{b(\Psi_{B_{1g}}^4 + \Psi_{B_{2g}}^4)}{2} + c\Psi_{B_{1g}}^2\Psi_{B_{2g}}^2.$$

Here, we realize that the assumption $c \approx b$ allows for a convenient reparametrization of the order parameters:

$$\begin{pmatrix} \Psi_{B_{1g}} \\ \Psi_{B_{2g}} \end{pmatrix} = \begin{pmatrix} \Psi_0 \cos(\varphi) \\ \Psi_0 \sin(\varphi) \end{pmatrix}, \quad (14)$$

where Ψ_0 represents a total order magnitude and φ an angle that defines the mixing of the two components. The minimization of the proposed Landau model with respect to Ψ_0 determines that the spin order $\Psi_0 = \sqrt{a(T - T_{\text{SO}})/b}$ sets in strictly at T_{SO} irrespective of the component mixing angle φ . The crucial difference from the single component model is that we must include all the strain-coupling to the lowest order of $\Psi_{B_{1g}}$ and $\Psi_{B_{2g}}$:

$$F_{\Psi_{B_{1g}}} = \alpha_{11}\epsilon_{A_{1g};1}\Psi_{B_{1g}}^2 + \alpha_{21}\epsilon_{A_{1g};2}\Psi_{B_{1g}}^2 + \beta_{21}\epsilon_{B_{2g}}^2\Psi_{B_{1g}}^2 + \beta_{11}\epsilon_{B_{1g}}\Psi_{B_{1g}}, \quad (15)$$

$$F_{\Psi_{B_{2g}}} = \alpha_{12}\epsilon_{A_{1g};1}\Psi_{B_{2g}}^2 + \alpha_{22}\epsilon_{A_{1g};2}\Psi_{B_{2g}}^2 + \beta_{12}\epsilon_{B_{1g}}^2\Psi_{B_{2g}}^2 + \beta_{22}\epsilon_{B_{2g}}\Psi_{B_{2g}}, \quad (16)$$

where coefficients α_{ij} define coupling strength to the symmetric, and β_{ij} to the asymmetric strain (we take the first index i to refer to the strain component, e.g., $i = 1 \rightarrow \epsilon_{A_{1g},1}$, and second index j to refer to the symmetry of the order parameter). The spin-structure coupling and the elastic energy contribution are left unchanged.

With the introduction of the order parameter reparametrization and the minimization of the free energy with respect to Ψ_0 , in case of the $\sigma_{[110]}$ strain, we get:

$$\Delta T_{\text{SO}}(\sigma_{[110]}, \varphi) = [f(\alpha_{11}, \alpha_{21}) \sin^2 \varphi + f(\alpha_{12}, \alpha_{22}) \cos^2 \varphi] \sigma_{110} - \frac{\beta_{12} \cos^2(\varphi)}{G_{xy}^2 a} \sigma_{110}^2. \quad (17)$$

We have already demonstrated that the suppression rate $f(\alpha_{12}, \alpha_{22})$, related to the $\Psi_{B_{2g}}$ spin order, vanishes, but one should not assume the same for $f(\alpha_{11}, \alpha_{21})$ rate. Nevertheless, by fitting the quadratic function to our measurements, we can show that the quadratic suppression constant β_{eff} is indeed reduced by some factor $\cos^2 \varphi$. Finally, more experimental data is needed to get the exact dependence of the mixing angle φ on the orientation of the applied in-plane magnetic field. However, by looking at the crystal symmetry, we must assume that the model is symmetric to rotation by $\phi = 90^\circ$ when the spin stripe direction coincides again with CuO bonds. In order to correlate the model to the structure, in the main article we use the reparametrization with $\varphi = 2\phi$.